Conference Paper, Published Version

Mitsui, Jun; Kubota, Shin-Ichi; Matsumoto, Akira

Stability of Armor Units Covering High-Mound Composite Breakwaters against Tsunami Overflow

Coastal Structures 2019 - Nils Goseberg, Torsten Schlurmann (eds) - © 2019 Bundesanstalt für Wasserbau
ISBN 978-3-939230-64-9 (Online) - DOI: 10.18451/978-3-939230-64-9_005

Stability of Armor Units Covering High-Mound Composite Breakwaters against Tsunami Overflow

J. Mitsui, S. Kubota & A. Matsumoto
Fudo Tetra Corporation, Ibaraki, Japan

Abstract: Stability of armor units covering high-mound composite breakwaters against tsunami overflow was examined. A series of hydraulic model experiments revealed that the main failure mode is the sliding of armor units on the slope due to fast flow along the mound. Installing large blocks at the toe of the mound was effective for improving stability. It was also confirmed that seepage flow reduced the stability of the blocks. Numerical analysis revealed that large hydraulic forces act on the blocks above the harbor-side water level while horizontal forces act a great deal less on the blocks near the seabed. This means that the height of the harbor-side water level greatly affects the stability of the blocks. Finally, an evaluation of the stability was performed based on the balance of the total forces acting on the blocks on the mound.

Keywords: Tsunami, Overflow, Armor units, Stability, High-mound composite breakwater

1 Introduction

In the design of breakwaters against tsunami, it is necessary to ensure the stability of armor units against tsunami. Many studies on the stability of armor units covering rubble mounds of composite breakwaters against tsunami overflow have been conducted since the 2011 Tohoku earthquake and tsunami, and knowledge has been accumulated. For example, Oi et al. (2012) showed that as the submerged water depth above the harbor-side mound becomes smaller, the impinging of the water jet onto the mound becomes more severe and the stability of the armor units decreases. Mitsui et al. (2014) proposed a stability estimation method for armor units covering rubble mound of composite breakwaters against tsunami overflow, and they incorporated the influence of submerged water depth above the mound as a parameter to determine the stability number used in the formulae. In these studies, it was shown that the lower the harbor-side water level, the more severe the impinging water jet onto the mound and the lower the stability of the armor units.

Although composite breakwaters are commonly constructed in Japan, sloping breakwaters or high-mound composite breakwaters with mounds higher than the water levels are often used at relatively shallow water depths such as within the surf zone (Tanimoto and Ojima, 1983). In such breakwaters, since the crest of the mound is above the water surface, and overflow water jets act directly on the armor units, it is assumed that more severe conditions will be encountered. Hasegawa et al. (2014) studied the stability of armor units against tsunami overflow for a breakwater installed on a coral reef where the armor units were partially dried out. Aniel-Quiroga et al. (2018) investigated rubble mound breakwaters against both the first impact of solitons and the subsequent overflow. However, few studies have been conducted under such conditions where mounds have dried out.

Therefore, in this study, hydraulic model tests and numerical analysis were carried out for the purpose of clarifying the failure mechanism of armor units against tsunami overflow targeting a high-mound breakwater where the harbor-side mound crest was above the still water level. First, in the hydraulic model experiments, the stability of armor units against a steady overflow of tsunami was investigated by changing the shape and mass of the armor units on the harbor-side mound. The failure modes of the armor units were observed, and effective stability improvement measures were also

investigated. In addition, the influence of the seepage flow through the mound on the stability of the armor units was studied. In the numerical analysis, the tsunami overflow situation in the hydraulic model experiments were reproduced, and the failure mechanism was discussed based on the fluid forces acting on the individual armor units. Finally, the evaluation of stability based on the calculated fluid force on each armor unit was attempted.

2 Hydraulic Model Experiments

2.1 Overview of Experiments

In the experiments, a circulating flow was generated in a water channel using a pump, and a steady overflow of tsunami was reproduced. A two-dimensional water channel with a length of 50 m, a width of 1.0 m and a height of 1.5 m was used. The setup in the water channel is shown in Fig. 1. A horizontal mortar seabed was partitioned into two sections along the length, and a breakwater model was installed in one 50 cm wide waterway. Water mass over the breakwater circulates from behind the partition wall. The model scale is 1/50. The typical cross section of the breakwater is shown in Fig. 2. The ground level at which the breakwater was installed is relatively shallow at -4.2 m (-8.4 cm in the model scale). A superstructure was installed on the rubble mound. The base of the superstructure was +2.0 m, and the crest height was +5.5 m. The seaside mound of the breakwater was covered with wave dissipating concrete blocks. For the rubble mound, 300 to 1000 kg / piece (2.4 to 8.0 g / piece in model scale) of stones were used. Armor units were installed on the harbor-side as a countermeasure against tsunami overflow. Two kinds of flat-type armor units as shown in Fig. 3 were used for the harbor-side armor units. The X-block is a flat-type armor block widely used in Japan for covering the rubble mounds of breakwaters. The Permex is an armor block developed based on the X-block, which has high stability against waves from the five holes provided in the block (Hamaguchi et al., 2007). The experiments were conducted by changing the shape and mass of the armor units as shown in Tab. 1.

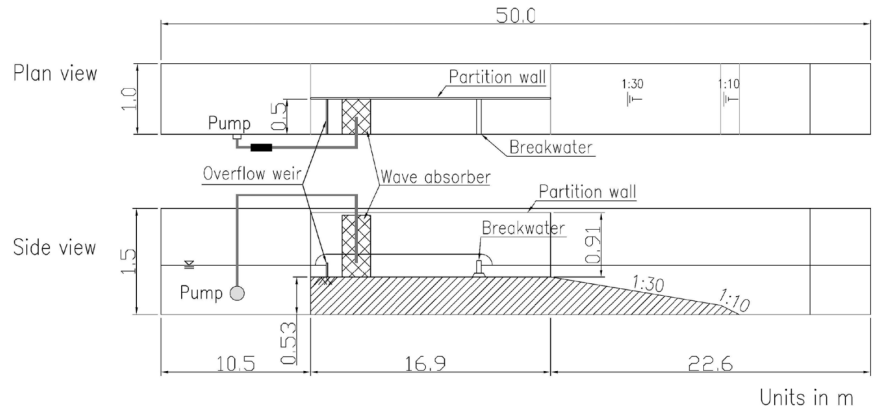

Fig. 1. Test setup in the water channel.

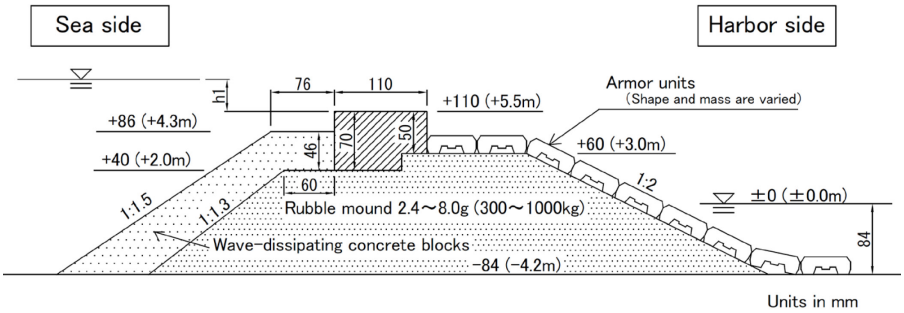

Fig. 2. Typical cross section of the tested breakwater. Units in mm (the values in parentheses indicate the values converted to the prototype scale).

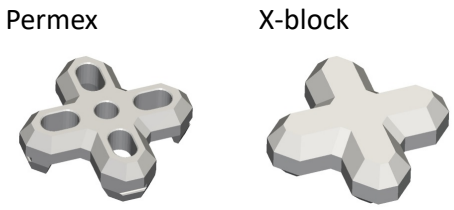

Fig. 3. Armor units used in the experiments.

Tab. 1. Test cases. The values in parentheses indicate the values converted to the prototype scale. N_{crest} is a number of blocks at the crest of the mound.

Case	Armor units			N_{crest}	Note
	Type	Mass	Density		
1	Permex	32.6 g (4.1 t)	2.3 g/cm^3	2	
2		64.6 g (8.1 t)			
3		128.8 g (16.1 t)			
4		145.6 g (18.2 t)	2.6 g/cm^3		
5		64.6 g (8.1 t)	2.3 g/cm^3	4	
6	X-block	129.8 g (16.2 t)		2	
7		244.2 g (30.5 t)			
8	Permex	64.6 g (8.1 t)			Reinforced against sliding using additional blocks
9					Only overflow is applied
10					Only seepage flow is applied

A steady overflow of tsunami was applied for 15 minutes in the prototype scale (127 seconds in the model scale). The stability limit of the armor units was investigated by gradually raising the seaside water level in 0.5 m increments (1 cm in the model scale) with the harbor-side water level kept at ± 0 m. After the pump was operated and steady state overflow was applied, the pump was stopped once and the behavior of the blocks observed, and then the next tsunami rank was applied. At that time, the armor units were not rebuilt, and the tsunami for the next rank was subsequently operated. Adjustment of the water level was performed by the flow rate of the pump and the initial water level in the water channel. These conditions were determined by the preliminary test.

In order to obtain the flow rate of the seepage flow passing through the mound, measurement of the seepage flow rate was separately conducted. Seepage flow was generated alone without overflow by installing a screen at the top of the breakwater. The flow rate was obtained by measuring the cross-sectional mean flow velocity behind the breakwater. The flow velocity was measured using an electromagnetic current meter at intervals of 1 cm in the height direction with 5 measurement lines in the width direction. The harbor-side water level was fixed at ± 0 cm, and the seaside water level was varied to four conditions of +7 cm, +14 cm, +21 cm, and +28 cm. The relationship between the water level difference and the seepage flow rate was then obtained.

2.2 Failure mode of the armor units and stability improvement measures

When the pump was operated and the seaside water level rose, the water level in the mound rose accordingly, and by the time the overflow started, the inside of the mound had become fully filled with water. From this time, seepage flow through the mound flowing out of the mound surface was observed. When the seaside water level rose further and overflow started, the water mass over the superstructure dropped to the crest of the harbor-side mound and flowed down the mound slope in a supercritical flow.

The stability test results for each case are described below. In Cases 1 to 4, masses of 32.6 g, 64.6 g, 128.8 g, and 145.6 g of Permex were used. The situation after the tsunami action in each case is shown in Fig. 4. The 32.6 g and 64.6 g blocks were damaged at an overflow depth h_1 of 3 cm, and the 128.8 g and 145.6 g blocks were damaged at an overflow depth h_1 of 4 cm. Here, the overflow depth h_1 is defined as the difference between the seaside waver level and the crest height of the breakwater. The results of Cases 1 to 4 show that the stability tends to be improved by increasing the block mass and density, but the effect is not so large. In all the cases, all the armor units on the slope slid together

as shown in Fig. 5. It was observed that the sliding did not progress gradually, but occurred rapidly when the external forces exceeded a certain limit.

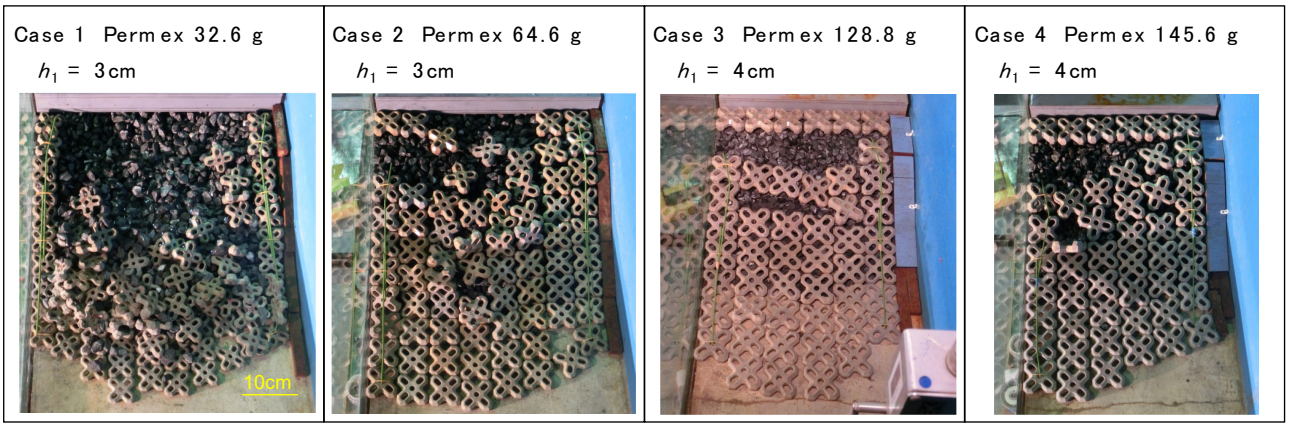

Fig. 4. Test results of Cases 1, 2, 3, and 4.

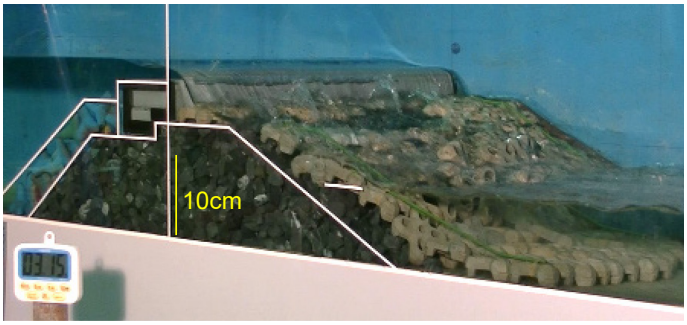

Fig. 5. Typical failure situation due to sliding of all the armor units on the slope (Case 2).

In Case 5, the crest width of the harbor-side mound was expanded by changing the number of armor units on the crest of the mound from 2 to 4. Permex of 64.6 g were used in this case. This is intended to improve the stability against sliding by moving the blocks on the slope away from the impingement position of the overtopped water. However, damage occurred at the same overflow depth as in the condition of 2 rows on the crest, and the failure mode was sliding (Fig. 6). It is shown that the failure mode of armor units when an overtopped water jet impinges on the crown section is overturning mode in normal composite breakwaters (Mitsui *et al*, 2014). Therefore, it is a feature of high-mound composite breakwaters that the failure mode is limited to sliding.

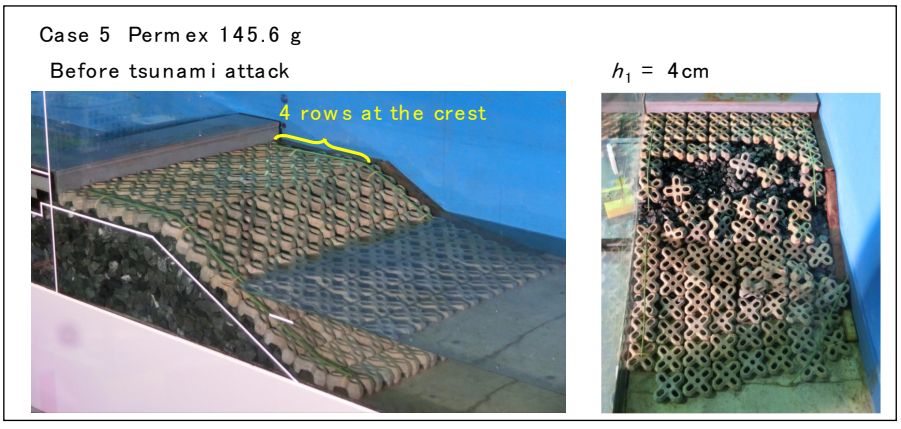

Fig. 6. Test results of Cases 5.

In Cases 6 and 7, X-blocks were used. Blocks with mass of 129.8 g were damaged at an overflow depth of 3 cm and blocks with mass of 244.2 g were damaged at an overflow water depth of 4 cm (Fig. 7). Compared with the results for Permex of the same mass, damage occurs at a lower tsunami height in X-block. Therefore, it was found that the stability of the armor units with holes is higher, as in the case of normal composite breakwaters.

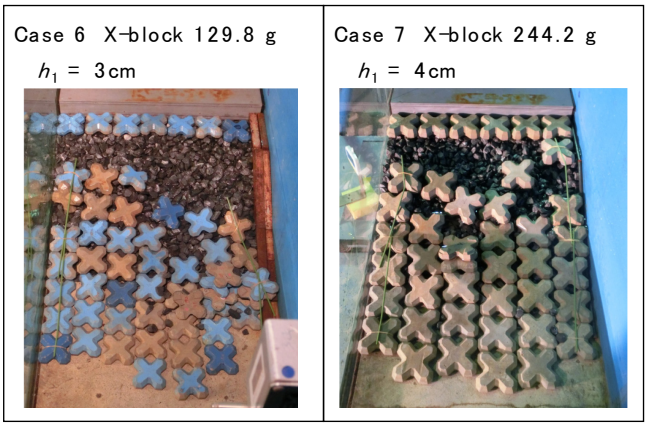

Fig. 7. Test results of Cases 6 and 7.

In Case 8, Permex with mass of 64.6 g were used to cover the mound and 2 rows of X-block with mass of 244.2 g were additionally placed on the toe as reinforcement against sliding. As shown in Fig. 8, it was stable to the overflow depth of 4 cm, which was the highest stability in all the cases.

Regarding the measure to improve stability, it was found that the installing large blocks at the toe of the mound is more effective to suppress sliding than enlarging individual blocks.

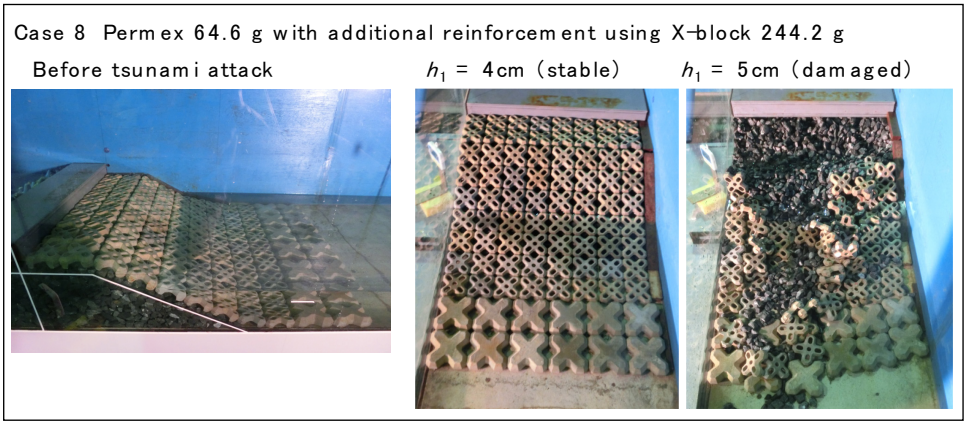

Fig. 8. Test results of Case 8.

2.3 *Influence of seepage flow*

It is thought that the seepage flow affected the stability of the armor units because the tested breakwater in this study had relatively short penetration distance in the mound and relatively large mound thickness. Therefore, additional experiments regarding the effect of seepage flow were conducted. In Case 9, only overflow was applied by covering the seaside mound surface with the impermeable sheet. In Case 10, only seepage flow was applied by installing a screen at the top of the breakwater. Schematic diagrams of the experimental conditions are shown in Fig. 9. In the experiment where only the seepage flow acted (Case 10), the flow rate of the pump was gradually increased, and the harbor-side water level was gradually raised until the armor units were damaged. In these cases, Permex with mass of 64.6 g were used.

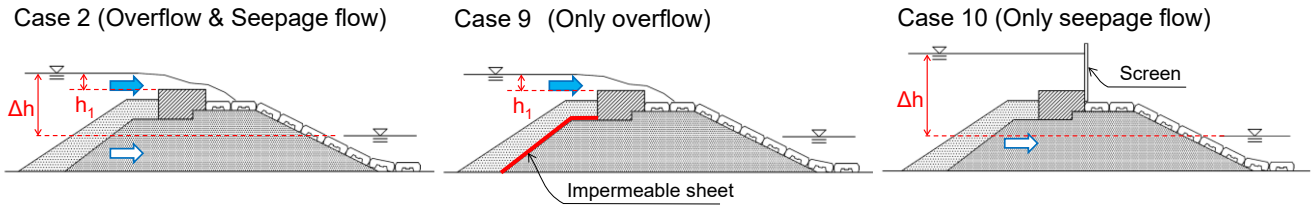

Fig. 9. Schematic diagrams of experiments on the influence of seepage flow.

Damage to armor units occurred by sliding of the blocks in both Case 9 and Case 10. In Case 9 where the mound was impermeable and only overflow was applied, damage occurred at an overflow depth of 4 cm. It was confirmed that the stability of the armor units is reduced by the seepage flow as the overflow depth at the sliding limit increased slightly compared to the normal condition (Case 2), where damage occurred at the overflow depth of 3 cm. In Case 10, where only seepage flow applied, damage occurred when the water level difference between the inside and outside of the breakwater reached 30.5 cm.

Next, the flow rates due to overflow and seepage flow at the occurrence of damage were calculated. First, the overflow discharge was estimated by the Hom-ma formula (Hom-ma, 1940) as shown below.

$$q_{overflow} = 0.35h_1\sqrt{2gh_1} \quad (1)$$

where, $q_{overflow}$ is the overflow discharge per unit width, and g is the gravity acceleration. The seepage flow discharge $q_{seepage}$ was estimated as shown in Eq. (2) by the regression equation obtained from the relationship between the water level difference Δh and the seepage flow discharge measured under several conditions.

$$q_{seepage} = -0.0532\Delta h^2 + 5.2254\Delta h \quad (2)$$

The overflow discharge and seepage flow discharge at the stability limit are shown in Tab. 2 and Fig. 10. The results show that the sum of the overflow and the seepage flow discharge q_{sum} at the stability limit is comparable in all cases. This fact suggests that the total flow rate of the overflow and seepage flow discharge determines the fluid forces on the blocks on the slope, and the difference in the flow path is not important.

Tab. 2. Overflow discharge and seepage flow discharge at the stability limit.

	h_1 at stability limit (cm)	Δh at stability limit (cm)	$q_{overflow}$ (cm^2/s)	$q_{seepage}$ (cm^2/s)	q_{sum} (cm^2/s)
Case 2 (overflow & seepage flow)	2 – 3	13 – 14	44 – 81	59 – 63	103 – 143
Case 9 (only overflow)	3 – 4	-	81 – 124	0	81 – 124
Case 10 (only seepage flow)	-	30.5	0	110	110

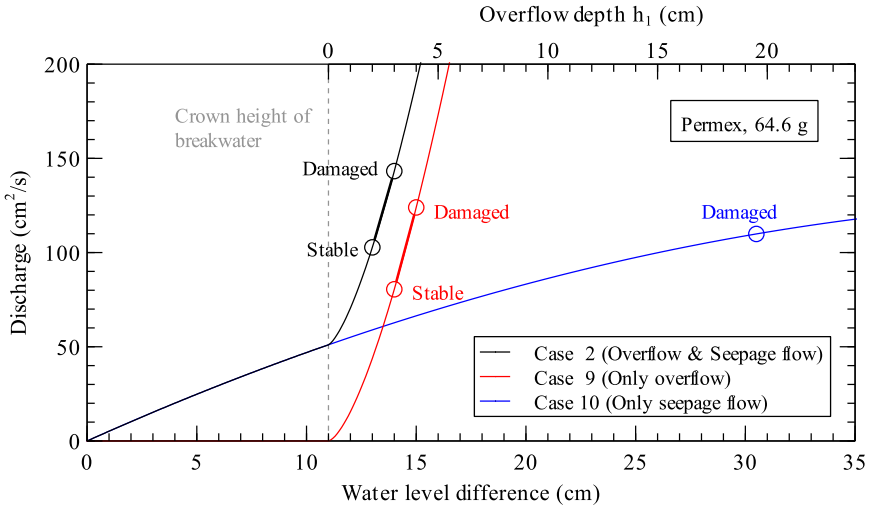

Fig. 10. Overflow discharge and seepage flow discharge at the occurrence of damage.

3 Numerical Analysis

3.1 Methods

In order to clarify the details of the damage mechanism in the armor units, the hydraulic model experiment was reproduced using numerical analysis. The fluid force acting on each block and the pressure distribution in the mound were examined. Case 2 using Permex with mass of 64.6 g was reproduced by the numerical analysis. The harbor-side water level was constant at ± 0 cm as in the experiment, and the overflow depth was changed to 2 cm, 3 cm, and 4 cm.

An open source CFD software OpenFOAM (version 2.4.0) was used for the numerical analysis. The solver named OlaFlow (Higuera *et.al*, 2014) which is an extended version of the VOF solver for gas-liquid two-phase flow based on a porous model was used. The computational domain was 8 m in length centering on the breakwater) and 3.1 cm in width (half the block length) in consideration of the symmetry of the shape of the armor unit. The steady overflow was generated by inflowing a constant flow from the seaside end of the computational domain and outflowing with the same flow rate from the harbor-side end of the computational domain.

Since it can be regarded as an almost uniform phenomenon in the channel width direction except in the vicinity of the armor units, the computational grid in the width direction is divided only around the armor unit. The three-dimensional shape of the armor unit was reproduced. The grid size around the armor unit is about 1 mm, which is about 1/60 of the block length. The fluid forces acting on the armor units were obtained by integrating the pressure on the block surface.

The rubble mound and the wave-dissipating concrete blocks installed on the seaside of the breakwater were modeled as porous bodies. The momentum conservation law in this numerical model is given by the following equation.

$$(1+c)\frac{\partial}{\partial t}\frac{\rho u_i}{n}+\frac{u_j}{n}\frac{\partial}{\partial x_j}\frac{\rho u_i}{n}=-\frac{\partial}{\partial x_i}p+\rho g_i+\frac{\partial}{\partial x_j}\left(\mu\frac{\partial}{\partial x_j}\frac{u_i}{n}\right)-A\frac{u_i}{n}-B\frac{u_i}{n}\left|\frac{u_i}{n}\right| \tag{3}$$

in which, ρ is the density, u_i is the flow velocity vector, p is the pressure, μ is the viscosity coefficient, n is the porosity, and c is the coefficient of inertia, and we used c = 0.34 according to previous research (Higuera *et.al*, 2014). Also, A and B are coefficients related to the resistance received from the porous body. They are expressed by the following equation (Engelund, 1953).

$$A=\alpha\frac{(1-n)^3}{n^2}\frac{\mu}{D_{50}^2},\ B=\beta\frac{1-n}{n^2}\frac{\rho}{D_{50}} \tag{4}$$

where, D_{50} is the mean nominal diameter, and α and β are the material constants. The material constants α and β of the rubble mound and the wave-dissipating concrete blocks were determined by calibration in advance so that the seepage flow rate agreed with the experimental value. Tab. 3 shows the material constants and physical properties used for the calculation.

Tab. 3. Material constants and physical properties of the rubble mound and the wave-dissipating concrete blocks.

	Wave-dissipating concrete blocks	Rubble mound
D_{50} (mm)	23.4	14.6
n (%)	50.0	39.7
α	50	500
β	0.6	2.0

3.2 Analysis Result and Discussion

3.2.1 Characteristics of the Flow Field

Fig. 11 shows the result of numerical analysis under an overflow depth of 3 cm where the armor units were damaged in the experiment. The overtopped water jet fell on the blocks on the crest of the mound and flowed down along the mound slope. Also, it can be seen that a relatively fast flow occurs near the harbor-side water surface, and there is almost no flow near the seabed. From the contour of the piezometric head in the mound, it can be read that a nearly uniform horizontal hydraulic gradient

has been generated from the lower part of the superstructure to the harbor-side. It shows that the seepage flow is generated in the horizontal direction.

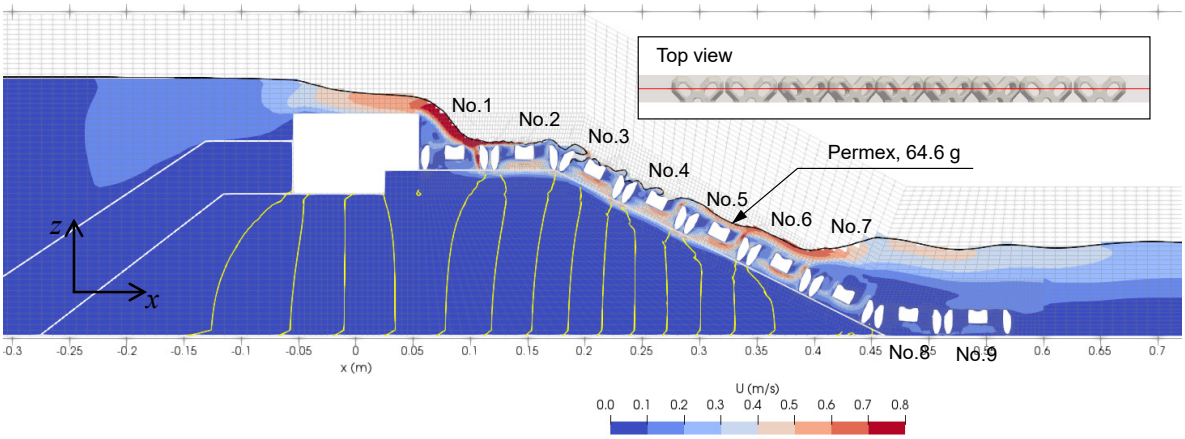

Fig. 11. Flow velocity and pressure distribution obtained by numerical computation. The colors red and blue indicate the flow velocity. The yellow lines show the contours of the piezometric head in the rubble mound with increments of 0.01 m.

3.2.2 Fluid Forces Acting on the Armor Units

The calculated horizontal and vertical fluid forces F_x and F_z acting on each block are shown in Fig. 12. The figure shows that a large horizontal force is acting from the top of the slope to the vicinity of the still water level. On the other hand, it is clear that the horizontal force acts only slightly on the blocks near the seabed, and only the buoyancy force acts upward. Therefore, the blocks above the water level act in the direction to cause sliding, and the blocks below the water level act as resistance. This is consistent with the experimental results that installing additional blocks at the toe of the mound is effective to suppress sliding. In the case of conventional composite breakwaters, the location receiving a large fluid force is usually limited to the vicinity of the impinging position of the overflow jet. On the other hand, in the case of a high-mound composite breakwater, the fluid force near the impinging position of the water jet is not always the largest, and a large fluid force acts over a relatively wide area on the still water level. From such characteristics of fluid force, since the range of occurrence of large fluid force changes depending on the harbor-side water level, it is thought that the height of the harbor-side water level greatly affects the stability of the armor units.

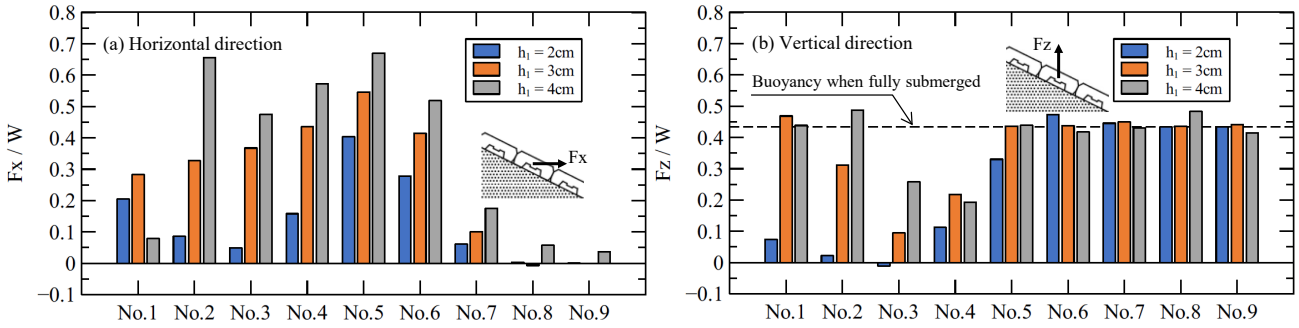

Fig. 12. Calculated horizontal and vertical fluid forces acting on each block. Fluid forces are shown divided by block weight W.

3.2.3 Stability Evaluation of Armor Units Based on Calculated Fluid Forces

The evaluation of the stability of armor units was attempted based on the calculated fluid force on each armor unit. The stability against sliding was evaluated by considering the balance of the forces of the whole block in the same way as in our previous study (Mitsui et al. 2015). First, the forces acting on the individual blocks were decomposed into a normal direction and a tangential direction of the mound, and the sliding force F_{sld} and the resistance force F_{res} were obtained by the following equations.

$$F_{sld} = W \sin\theta + F_x \cos\theta + F_z \sin\theta \quad (5)$$

$$F_{res} = \mu\{W \cos\theta - (F_x \sin\theta + F_z \cos\theta)\} \quad (6)$$

where, W is the weight in air of the armor unit, θ is the installation angle of the armor unit, and μ is the friction coefficient. It should be noted that the buoyancy is included in the calculation result of the fluid forces. In this study, resistance due to interlocking between the blocks and the stones was included in the friction force, and the value of the coefficient μ was set to 1.0 according to our previous study (Mitsui et al. 2015). The friction coefficient of the blocks at the toe of the mound was set to 0.6 considering that a mortar seabed was used in the experiments. Tab. 4 shows the calculation results of the sliding forces F_{sld} and resistance forces F_{res}. The bold numbers in the table indicate that the sliding force exceeds the resistance force. For example, when the overflow depth is 3 cm, the sliding forces exceed the resistance forces in the blocks from No. 3 (top of the slope) to No. 6 (near the harbor-side water level), and the resistance forces exceed in the blocks below No. 7 block. Therefore, the stability against sliding on the entire slope can be evaluated by comparing the sum of the acting forces and the resisting forces for the range below the No. 3 blocks. The safety factor SF is also shown in the table which is calculated as the sum of the resistance forces divided by the sum of the sliding forces. This means that the armor blocks will not slide if the safety factor is larger than 1. The safety factor is less than 1 under the condition of an overflow depth 3 cm or more, which is consistent with the experimental results. It should be noted that the blocks No. 1 and No. 2 were also moved (see Case 2 in Fig. 4) in the experiment, but this is thought to be because the movement of blocks and rubble stones are not considered in this analysis. It was shown that the stability could be predicted based on the balance of the total forces acting on the blocks on the mound using the fluid force on each block calculated by numerical analysis.

Tab. 4. Calculated sliding forces F_{sld} and resistance forces F_{res}. The bold numbers indicate that the sliding force exceeds the resistance force.

Block No.	h_1 = 2 cm		h_1 = 3 cm		h_1 = 4 cm	
	F_{sld} (N)	F_{res} (N)	F_{sld} (N)	F_{res} (N)	F_{sld} (N)	F_{res} (N)
1	0.13	0.59	0.18	0.34	0.05	0.36
2	0.05	0.62	0.21	0.44	**0.42**	**0.33**
3	0.31	0.56	**0.46**	**0.41**	**0.48**	**0.29**
4	0.34	0.46	**0.47**	**0.32**	**0.55**	**0.29**
5	**0.42**	**0.26**	**0.47**	**0.16**	**0.54**	**0.13**
6	**0.31**	**0.22**	**0.39**	**0.20**	**0.46**	**0.18**
7	0.19	0.30	0.21	0.28	0.26	0.27
8	0.03	0.36	0.03	0.36	0.07	0.32
9	0.00	0.21	0.00	0.21	0.02	0.22
Safety factor SF	1.42 (No.5 – No.9)		0.96 (No.3 – No.9)		0.73 (No.2 – No.9)	

4 Conclusions

The main conclusions of this study are as follows:

(1) The main failure mode is the sliding of all blocks on the slope due to fast flow along the mound.

(2) It is effective to suppress sliding by installing large blocks at the toe of the mound rather than enlarging the individual blocks.

(3) It was confirmed that seepage flow reduces stability of armor blocks.

(4) Large horizontal fluid forces act on blocks above the harbor-side water level, while horizontal forces act much less on the blocks near the seabed. Therefore, the height of the harbor-side water level greatly affects the stability of the blocks.

(5) Using the fluid force on each block obtained by numerical computation, the stability against sliding could be predicted based on the balance of the total forces acting on the blocks on the mound.

References

Aniel-Quiroga, Í., Vidal, C., Lara, J.L., González, M, Sainz, Á., 2018. Stability of rubble-mound breakwaters under tsunami first impact and overflow based on laboratory experiments. Coastal Engineering, Elsevier, 135, 39-54.

Engelund, F., 1953. On the laminar and turbulent flow of ground water through homogeneous sand. Transactions of the Danish Academy of Technical Sciences 3.

Hamaguchi, M., Kubota, S., Matsumoto, A., Hanzawa, M., Yamamoto, M., Moritaka, H., Shimosako, K., 2007. Hydraulic stability of new flat type armor block with very large openings for use in composite breakwater rubble mound protection, in: Proceedings of 5th Coastal Structures International Conference, CSt07, Venice, Italy, 116-127.

Hasegawa, I., Tanaka, S., Yasuda, M., Yoshihira, K., Maesato, T., 2014. Stability of a breakwater on coral reef against tsunami. Journal of JSCE, Ser. B3 (Ocean Engineering), 70 (2), I_426-I_431 (in Japanese).

Higuera, P., Lara, J.L., Losada, I.J., 2014. Three-dimensional interactions of waves and porous coastal structures using OpenFOAM. Part I: Formulation and validation. Coastal Engineering, Elsevier, 83, 243-258.

Hom-ma, M., 1940. Discharge coefficient on overflow weir (part-2). JSCE Magazine, Civil Engineering, 26 (9), 849-862 (in Japanese).

Mitsui, J., Matsumoto, A., Hanzawa, M., Nadaoka, K., 2014. Stability of armor units covering rubble mound of composite breakwaters against a steady overflow of tsunami, in: Proceedings of 34th International Conference on Coastal Engineering, Seoul, Korea, structures.34.

Mitsui, J., Matsumoto, A., Hanzawa, M., Nadaoka, K., 2015. Numerical analysis on tsunami overtopping caisson breakwaters and stability of armor units, in: Proceedings of Coastal Structures and Solutions to Coastal Disasters 2015: Tsunamis, Boston, USA, 176-186.

Mitsui, J., Shin-ichi, K., Matsumoto, A., 2018. Stability estimation method for armor units for breakwaters with parapets against tsunami overflow, in: Proceedings of 36th International Conference on Coastal Engineering, Baltimore, Maryland, papers.26.

Oi, K., Hayashi, K., Kawano, S., 2012. Experimental study on reinforcement of coastal dikes and breakwaters for over flow in tsunami. Journal of JSCE, Ser. B3 (Ocean Engineering), 68 (2), I_96-I_101 (in Japanese).

Tanimoto, K., Ojima, R., 1983. Experimental study of wave forces acting on superstructure of sloping breakwaters and on block type composite breakwaters. Technical note of the Port and Harbour Research Instutute Ministry of Transport, Japan, No. 450, 32p (in Japanese).